

Modeling and Analysis on Exploration Rover with Screw Drive Mechanism over Loose Soil

Kenji Nagaoka*, Takashi Kubota**

*The Graduate University for Advanced Studies (Sokendai), Japan
e-mail: nagaoka@nsl.isas.jaxa.jp

**Institute of Space and Astronautical Science, JAXA, Japan
e-mail: kubota@isas.jaxa.jp

Abstract

This paper describes the mathematical modeling and the propulsion characteristics of a mobile robot driven by an Archimedean screw units, called Screw Drive Rover. In order to realize secure locomotion on loose soil, it is a serious issue for conventional wheeled or tracked locomotion to get stuck in the soil due to a slippage. On this point, the proposed rover is expected to be of robustness to this issues. Furthermore, the rover can also travel in various directions by using two screw units. However, the interaction between such a screw unit and the soil is quite complicated, and therefore, its detail remains undefined. This paper attempts to predict the tractive effort of Screw Drive Rover on loose soil. To accomplish the theoretical analyses, the mathematical modeling is newly developed based on soil-screw interactive mechanics. Finally, the validity of the model is demonstrated by simulations.

1 Introduction

Through recent space explorations, traveling or cruising technology on an extraterrestrial surface has played a significant role for mission successes. Recently the Mars Exploration Rovers (MERs) demonstrated by NASA have performed impressive achievements on Mars [1]. MERs employ six wheels for locomotion on the martian terrain, and until now these rovers have acquired scientific findings for more than six years. In the meantime, a certain limitation of wheeled locomotion on loose soil has come to light through the MER mission. Actually, MER Spirit has been stuck in a sand trap [2], and then the rover team eventually gave up on its extrication. In consideration of this, more theoretical discussions are required for lunar and planetary exploration rovers to assure robust locomotion on loose soil such as lunar regolith [3]. As one promising approach for them, terramechanics investigating soil-vehicle interaction has received a lot of attention. However, the interactive mechanics is fundamentally addressed based on semi-empirical static equations [4, 5, 6]. These equations are also comprised of some empirical pa-

rameters. Accordingly, it is practically difficult to dynamically control conventional wheeled or tracked robot on soil to avoid a serious stuck. Further to this, essential improvement of a locomotion mechanism should be also conducted to cope with such difficult terrain.

Humans have been interested in 'spirals' due to its geometric uniqueness in history [7]. Spiral structure has been applied in versatile applications. As one typical example, an Archimedean screw mechanism has been known as a screw-pump since early times [8]. So, the authors have proposed a mobile robot driven by such screw mechanism for traveling on loose soil. The proposed system is expected to be robust to slipping and getting stuck in loose soil because of the propulsive force in the axial direction of rotation. Combination of inclined screw blades also lead to movement in diverse direction. Furthermore, its structural simplicity would be one of the advantages as compared to a track. A screw driven vehicle like the proposed system, however, is not a new idea. In fact, screw drive amphibians [9, 10] have utilized since more than 170 years ago. And also, the screw locomotion was tried and tested when NASA developed the Lunar Roving Vehicles in Apollo missions [11]. To date, a small number of experimental studies on the screw vehicle have been also reported [12, 13, 14]. But the soil-screw interaction is still unknown, and theoretical approaches toward the understanding are extremely limited. Thus, the mathematical modeling of the soil-screw interaction becomes a new challenge to be elaborated because terramechanics has mainly targeted just a wheel and a track. Likewise, there have been several screw driven robots such as an *in vivo* robot for laparoscopy [15, 16], an endoscope [17] or a spiral-type magnetic micro-machine [18]. *In vivo* robots and swimming robots are typically moved by contact with viscoelastic biological tissue and incompressible viscous fluid, respectively. Although they are equipped with the similar mechanism for locomotion, their targeted environments are quite different from terrain. Naturally, the respective models also differ on theoretical grounds.

From the foregoing considerations, this study focuses on the derivation of the novel soil-screw interaction

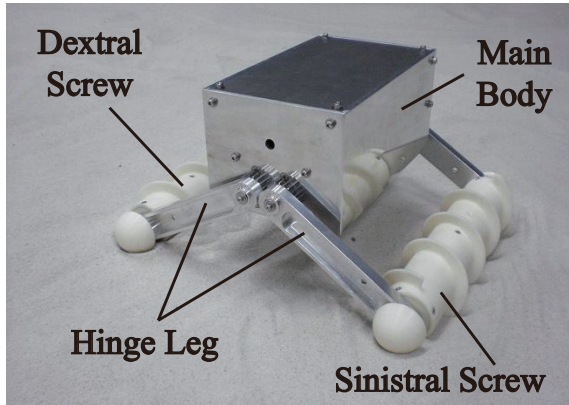


Figure 1. Schematic of Screw Drive Rover

model. As the first step, this paper addresses in particular the interaction modeling based on conventional soil-wheel model in terramechanics. In this paper, unlike the typical wheel or track models, three-dimensional screw helical motion is newly considered. Characteristics of the developed model are elaborated by numerical simulations.

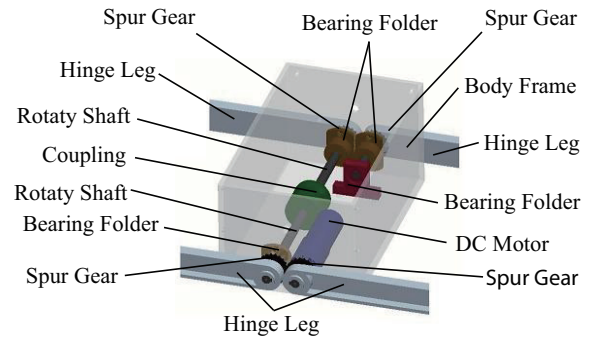
2 Proposition of Screw Drive Rover System

2.1 Configuration and Ideal Mobility

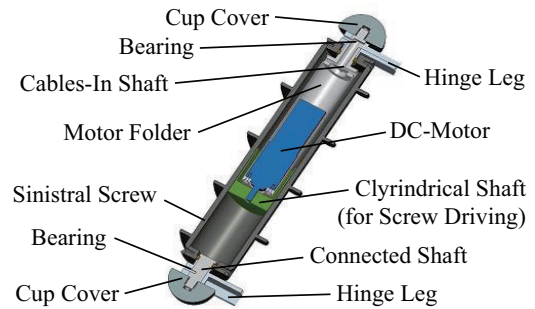
A novel rover equipped with Archimedean screw drive units, called Screw Drive Rover, has proposed to achieve better locomotion on loose soil. Screw Drive Rover is composed of a main body, hinge legs, and sinistral and dextral screw units winding N -times around each cylinder, where the screw thickness is considered as a negligibly small value. In particular, this rover is able to drive the hinge legs in synchronization to improve geometrically its stability. The authors have elaborated the mobility performance by applying the ideal kinematic model so far [19]. Of particular note is that the modeled Screw Drive Rover is capable of locomotion in diverse moving directions by using just two driving units.

2.2 Laboratory Tests

The authors have developed the Screw Drive Rover prototype to investigate briefly its empirical mobility on sand. Prior to the theoretical discussion, laboratory tests have been conducted by using the prototype. Schematic of the prototype is shown in Figure 1. The screw units are 12.5mm in height and 55mm in outer diameter of screw's cylinder, and the screw slope angles are 16deg with $N = 4$. The total system weights 6.4kg except for circuits and batteries. The overall configuration is approximately 200mm in height, 300mm in width and 300mm in longitudinal length. Additionally, each screw unit can be driven independently by DC motors and thus diverse locomotive directions are achieved as shown in Figure 2.



(a) Internal structure of main body and hinge legs



(b) Cross-section diagram of screw drive unit

Figure 2. Mechanical structure of Screw Drive Rover

The results of the basic traveling tests on the test sand, which is quartz sand, are shown in Figure 3. From the results, it is confirmed that Screw Drive Rover can realize multi-directional locomotion on sandy terrain by the two screw units. Furthermore, in some cases locomotion trajectories of the ideal model are different from ones of the tests. Hence, a more practical model is needed for path following or tracking control of Screw Drive Rover.

2.3 Challenge and Motivation

On the basis of the previous traveling tests and the ideal modeling, the development of a mathematical model with the soil mechanics would appear to be a next challenge. So, the interactive mechanics model between the soil and the screw is derived based on terramechanics. Then, the simulated tractive performances of Screw Drive Rover are analytically discussed. The locomotion model would particularly become a nonholonomic system, and therefore, the modeling is of considerable significance for the achievement of desired movement.

3 Modeling of Soil-Screw Interaction

3.1 Preliminary

The motion states of Screw Drive Rover are preliminarily defined. Absolute coordinate system $\Sigma_O\{X, Y, Z\}$ is set as illustrated in Figure 4. The modeling assumes a

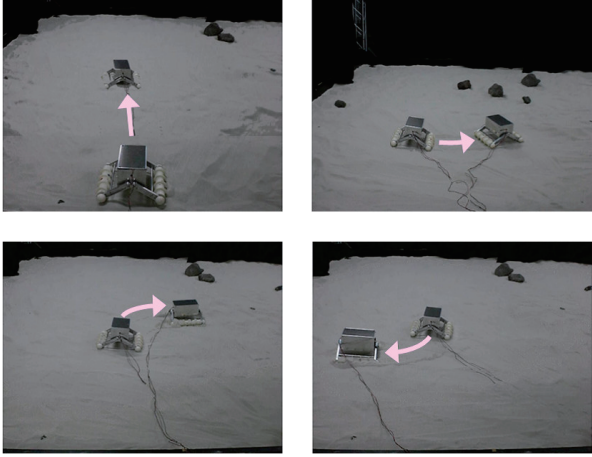


Figure 3. Diverse mobility performance demonstrated by Screw Drive Rover prototype on sand

family of soil-screw moving together as one body. Further to this, the screw model technically depends on its winding direction. But the definitions and formulas for the modeling can be essentially regarded as common expressions. Therefore, unified expressions are described for each screw unit unless stated otherwise.

3.2 Screw Geometry

First, the screw pitch and the slope angle are defined as p and η , respectively. These values are constant and represented at the midpoint between the cylinder surface and the screw blade edge. Here, p and η satisfy the following relation.

$$p = \pi(r + r_1) \tan \eta \quad (1)$$

where r_1 is the screw cylinder radius, r_2 is the screw blade's height and r is also defined as $r = r_1 + r_2$. Here, the screw length b is defined as $b = N \cdot p$.

The screw blade surface area, dA , at micro region $d\theta$ from the screw winding angle θ , can be approximated as follows.

$$dA(\theta) = \pi(r^2 - r_1^2) \cdot d\theta \quad (2)$$

The locomotion is basically governed by forces on dA .

3.3 Kinematic Definitions

The screw fixed coordinates $\Sigma_S\{x, y, z\}$ is first set to be the right-handed coordinate system with the x and y axis in the longitudinal and vertical directions of the screw unit. Figure 4 shows the kinematic model of the screw unit. Σ_S is defined as the rotating frame to Σ_O , which rotates around Z axis by δ . Here, robotic locomotion on soil is fundamentally accompanied with slip because of soil compaction and failure. Assuming the rover's attitude rotations around x and y axes are zero, the slip in x axis, s_x ,

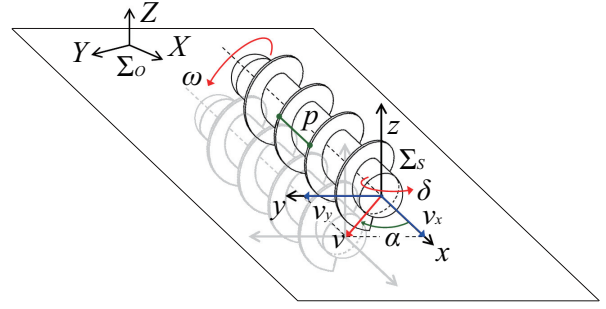


Figure 4. Kinematics of sinistral screw unit

is defined as follows [5, 14].

$$s_x = \begin{cases} \frac{p\omega/2\pi - v_x}{p\omega/2\pi} & \text{if } |p\omega/2\pi| \geq |v_x| \\ \frac{p\omega/2\pi - v_x}{v_x} & \text{otherwise} \end{cases} \quad (3)$$

where ω is the screw angular velocity, v_x is the velocity component in x direction, $0 \leq s_x \leq 1$ under a driving state and $-1 \leq s_x \leq 0$ under a braking state.

Direction of locomotion is defined. Given the velocity vector v in Σ_S , the angle between v and the x axis can be defined as slip angle α [20]. By the velocity components v_x and v_y in Σ_S , α is expressed as follows.

$$\alpha = \tan^{-1}(v_y/v_x) \quad (4)$$

On the contrary, v_x and v_y can be also written as a function of s_x and α .

$$v_x = \frac{p\omega(1 - s_x)}{2\pi}, \quad v_y = \frac{p\omega(1 - s_x)}{2\pi} \tan \alpha \quad (5)$$

3.4 Formulations of Contact Stress

3.4.1 Normal Stress

One of the significant subjects in the study of terramechanics is the relationship between normal stress σ and sinkage h . The relational angle expression is first given as follows [5, 23].

$$\theta_m = (c_1 + c_2 s_x) \theta_f \quad (6)$$

where c_1 and c_2 are coefficients depending on the soil-screw interaction. Technically, while the slip direction in Equation (6) does not necessarily correspond to s_x , the authors employ this relation like the conventional study on wheels [21].

Next, the normal stress distribution of the soil beneath the screw unit can be calculated as follows [5].

$$\sigma(\theta) = \begin{cases} \sigma_m \Theta_1^n & \text{if } \theta_m \leq \theta \leq \theta_f \\ \sigma_m \Theta_2^n & \text{otherwise} \end{cases} \quad (7)$$

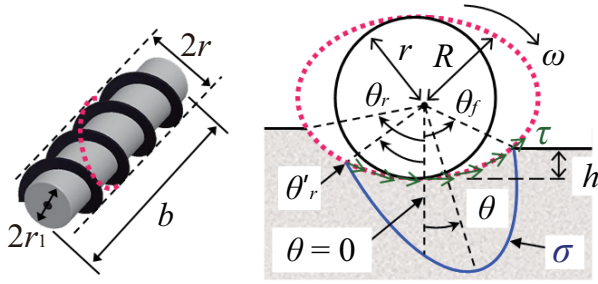


Figure 5. Interactive mechanics of soil and screw unit

and also,

$$\Theta_1(\theta) = \cos \theta - \cos \theta_f \quad (8)$$

$$\Theta_2(\theta) = \cos \left[\theta_f - \frac{\theta - \theta'_r}{\theta_m - \theta'_r} (\theta_f - \theta_m) \right] - \cos \theta_f \quad (9)$$

$$\sigma_m = (k_c/b + k_\phi) R^n \quad (10)$$

where θ is the screw angle ($\theta'_r \leq \theta \leq \theta_f$), $\theta'_r (\leq 0)$ is the effective exit angle, $\theta_f (\geq 0)$ is the entry angle, θ_m is the specific wheel angle at which the maximized normal stress occurs, b is the screw's longitudinal length, n is sinkage exponent, and k_c and k_ϕ are pressure-sinkage moduli regarding cohesion and internal friction, respectively. Let R be the elliptic distance as illustrated in Figure 5, and will be defined later on. Also, θ_f is geometrically derived by the following equation.

$$\theta_f = \cos^{-1} (1 - h/r) \quad (11)$$

In the conventional study in terramechanics, the condition $|\theta_r| \leq |\theta_f|$ is basically premised for the expression of σ beneath a rigid wheel. Figure 6 depicts the relationship between θ_f and h/r . This provides $h/r \approx 0.29$ at $\theta = 45^\circ$. On the other hand, in the case of the screw unit, $|\theta_f| \leq |\theta_r|$ has been observed through the traveling tests by the authors. This implies the reaction force from discharging soil is too small, and therefore, the stress distribution satisfying $|\theta_f| \leq |\theta_r|$ is obtained. So, this paper assumes $|\theta_f| \leq |\theta_r|$ by means of a transformation of θ_r to θ'_r . θ'_r achieving $|\theta'_r| \leq |\theta_f|$ is given as follows.

$$\theta'_r = -c_3 \theta_f \quad (12)$$

where $c_3 (\leq 1)$ is a positive angle coefficient.

The screw unit provides a elliptic cross section for discussing the normal and the shear stresses with angle θ as illustrated in Figure 5. In wheels, while the soil is sheared in elliptic trajectory when a wheeled vehicle steers, the common formula of the normal stress is applicable [20]. Hence, this paper also employs the unified normal stress distribution Equation (7).

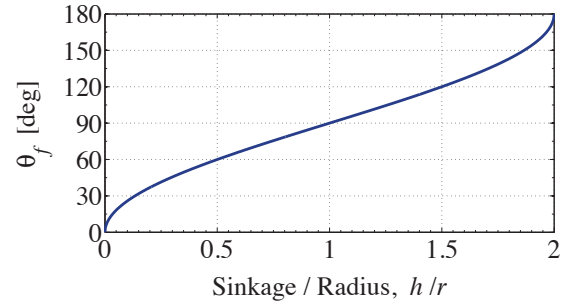


Figure 6. Relation between θ_f and h/r

3.4.2 Shear Stress

The shear stress of loose soil, τ , is generally formulated as follows [22].

$$\tau(\theta) = \tau_{\max} \cdot (1 - \exp^{-j/K}) \quad (13)$$

$$\tau_{\max}(\theta) = c + \sigma \tan \phi \quad (14)$$

where τ_{\max} is shear strength, ϕ is soil internal friction angle, c is soil cohesion, j is soil displacement and K is shear deformation modulus.

3.4.3 Shear Displacement of Soil

In this paper, unlike the traditional approaches of wheels, it is considered the soil between the screw blades move as one body with the blades. That is, the soil shear stress occurs along the outermost radius of the screw blade. Consequently, the three-dimensional expression of the screw's helical trajectory is needed for giving the soil thrust of the screw units by τ component. So this paper provides the screw motion trajectory in $\Sigma_O, \mathcal{T}(X, Y, Z)$, by the following expression.

$$\mathcal{T} = \begin{pmatrix} r \cos \theta \sin \delta + V_X t + X_0 \\ r \cos \theta \cos \delta + V_Y t + Y_0 \\ r \sin \theta + Z_0 \end{pmatrix}^T \quad (15)$$

and also,

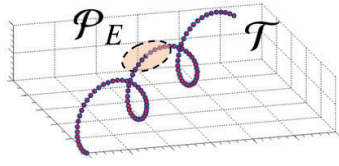
$$\begin{cases} V_X = v_x \cos \delta + v_y \sin \delta \\ V_Y = -v_x \sin \delta + v_y \cos \delta \end{cases} \quad (16)$$

where $(*)^T$ denotes matrix transposition.

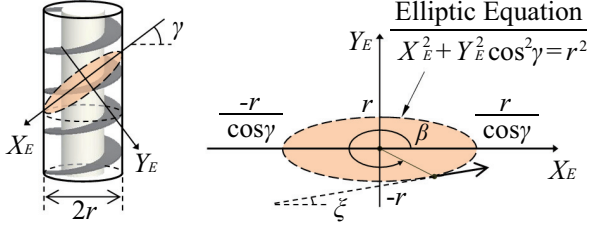
Then, the trajectory of the soil shearing is defined by angle $\gamma (= \pi/2 - \eta)$ as illustrated in Figure 7. This trajectory $\mathcal{P}_E(X_E, Y_E, Z_E)$ basically traces an ellipse. In the screw fixed elliptic coordinates $\Sigma_E\{X_E, Y_E, Z_E\}$, \mathcal{P}_E can be derived by β or $\theta (= \beta - 3\pi/2)$.

$$\mathcal{P}_E = \begin{pmatrix} \frac{r}{\cos \gamma} \cos \beta \\ r \sin \beta \\ 0 \end{pmatrix}^T = \begin{pmatrix} \frac{-r}{\cos \gamma} \sin \theta \\ r \cos \theta \\ 0 \end{pmatrix}^T \quad (17)$$

The tangential equation at a certain point $(x_a, -y_a)$ on



(a) Trajectories of screw blade and soil displacement



(b) Definition of soil shearing ellipse

Figure 7. Elliptic trajectory of soil shearing

\mathcal{P}_E is also represented as follows.

$$\frac{x_a}{r^2 \sec^2 \gamma} \cdot X_E + \frac{y_a}{r^2} \cdot Y_E = 1 \quad (18)$$

where x_a and y_a are positive values, and the sinkage is assumed to be less than r . Substituting Equation (17) into Equation (18), the above equation can be eventually simplified as follows.

$$y_a = -\frac{\cos \gamma}{\tan \beta} \cdot x_a + \frac{r \cos \gamma}{\sin \beta} \quad (19)$$

Accordingly, the inclination angle of the tangent, ξ , can be written as follows.

$$\xi = \tan^{-1}(-\cos \gamma \cdot \cot \beta) = \tan^{-1}(\cos \gamma \cdot \tan \theta) \quad (20)$$

Furthermore, the ellipse radius R can be formulated as a function of θ by

$$R(\theta) = r \sqrt{\cos^2 \theta + \sin^2 \theta \cdot \sec^2 \gamma} \quad (21)$$

As a result, j is defined as follows.

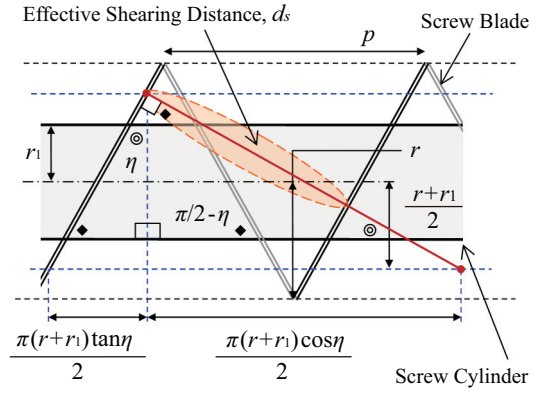
$$j(\theta) = \oint_{\mathcal{L}} v_j \cdot dt \quad (22)$$

and also,

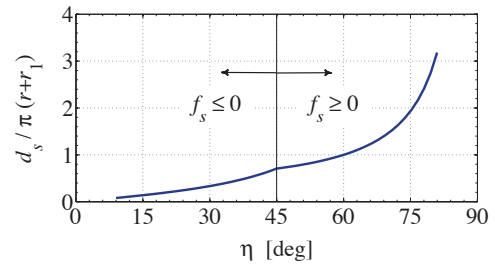
$$\mathcal{L} = \mathcal{T} + \mathcal{P}_O \quad (23)$$

$$\mathcal{P}_O = \begin{pmatrix} -r \sin \theta \cdot \sin(\delta + \gamma) \\ -r \sin \theta \cdot \cos(\delta + \gamma) \\ -r \sec \gamma \cdot \cos \theta \end{pmatrix}^T \quad (24)$$

where \mathcal{L} is the trajectory of the displaced soil in Σ_O and v_j is the relative soil displacement velocity along \mathcal{L} . Moreover, \mathcal{P}_O gives a transformation from \mathcal{P}_E , transforming



(a) Illustration of effective shearing distance



(b) Parametric analysis of d_s depending on η

Figure 8. Effective distance of soil shearing

their coordinates $\Sigma_E \rightarrow \Sigma_O$. In light of Equation (5), the time derivative of \mathcal{L} is given as follows.

$$\begin{aligned} \frac{d}{dt} \mathcal{L} &= \frac{d}{dt} (\mathcal{T} + \mathcal{P}_O) \\ &= \begin{pmatrix} \frac{p(1-s_x)}{2\pi} - r \cos \theta \sin \gamma \\ \frac{p(1-s_x)}{2\pi} \tan \alpha - r (\sin \theta + \cos \theta \cos \gamma) \\ r \cos \theta + \frac{r}{\cos \gamma} \sin \theta \end{pmatrix}^T \cdot \omega \\ &= \begin{pmatrix} \mathcal{L}_{v_{jx}} & \mathcal{L}_{v_{jy}} & \mathcal{L}_{v_{jz}} \end{pmatrix} \cdot \omega \end{aligned} \quad (25)$$

where δ and $\dot{\delta}$ are assumed to be zero.

Therefore, Equation (22) can be finally expressed as follows.

$$j(\theta) = \oint_{\mathcal{L}} v_j \cdot dt = \int_{\theta}^{\theta_f} \sqrt{\mathcal{L}_{v_{jx}}^2 + \mathcal{L}_{v_{jy}}^2 + \mathcal{L}_{v_{jz}}^2} \cdot d\theta \quad (26)$$

3.4.4 Stationary State of Dynamic Sinkage

On the basis of the study by Yamakawa *et al.* [24], the wheel's dynamic sinkage reaches a stationary state when the wheel drives with a constant slip. The stationary sinkage is ultimately proportional to the wheel slip, and the proportionality factor depends on both the wheel and the soil. So, this study assumes the following relationship in a similar way for subsequent simulation analyses.

$$h = h_0 + c_4 s_x \quad (27)$$

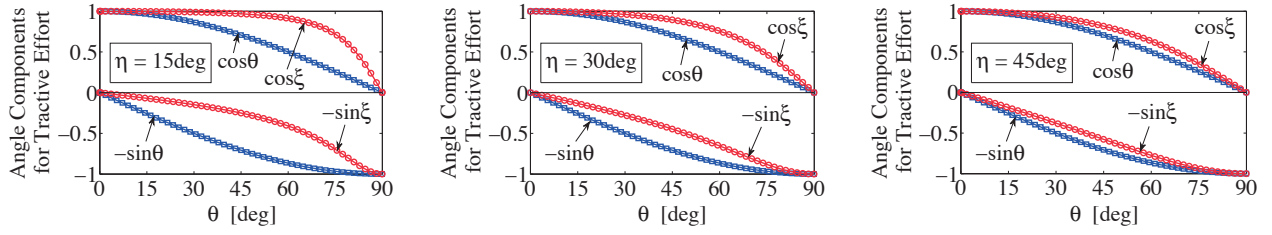


Figure 9. Angle components for tractive effort of stresses on circular and elliptic surfaces along angles

where h_0 is static sinkage before driving, c_4 is a positive coefficient. This enables us to simulate the relativity of the slip and the sinkage.

3.4.5 Soil Shearing Distance

The effective distance of the soil shearing, d_s , is geometrically constrained by η and p as illustrated in Figure 8(a). To evaluate the distance, the effective factor f_s is here given as follows.

$$f_s = \frac{p}{r_1} - \frac{\pi(r+r_1)(\tan\eta + \cot\eta)}{2r_1} \quad (28)$$

Thus, d_s is maximized with the positive f_s . Contrary to this, when f_s is negative, d_s is confined to the interscrew area. The positive f_s obviously appears at $45\text{deg} \leq \eta \leq 90\text{deg}$. Consequently, d_s can be introduced as follows.

$$d_s = \begin{cases} \frac{\pi(r+r_1)\tan\eta}{2\sin\eta} & \text{if } f_s \geq 0 \\ \frac{\pi(r+r_1)\tan\eta}{2\cos\eta} & \text{otherwise} \end{cases} \quad (29)$$

Figure 8(b) depicts the parametric characteristics of d_s pertaining to η . According to this, it can be confirmed d_s is strongly governed by η .

4 Synthetic Locomotion Model

4.1 Integrated Tractive Efforts

In accordance with the interaction model of the soil and the screw unit, the next is the introduction of the tractive efforts of Screw Drive Rover. The integrated tractive effort in x direction of Screw Drive Rover is defined as F_x and is calculated as follows.

$$F_x = \sum \text{sgn}(\omega) F \cos\eta \quad (30)$$

$$F = \iint (\tau \cos\xi - \sigma \sin\xi) dAd\theta \quad (31)$$

where \sum denotes the summation of the screw units. Let the integral region be determined based on d_s . Here, because the tractive effort is evaluated by whole integration, Equation (31) can be modified as follows.

$$F = b \cdot R \sin\eta \int_{\theta_f}^{\theta_j} (\tau \cos\xi - \sigma \sin\xi) d\theta \quad (32)$$

Likewise, the tractive effort in y direction is computed by

$$F_y = \sum \text{sgn}(\omega) F \sin\eta \quad (33)$$

where this paper assumes the body rotation δ is ignored as a primary analysis, giving $\delta = \dot{\delta} = 0$.

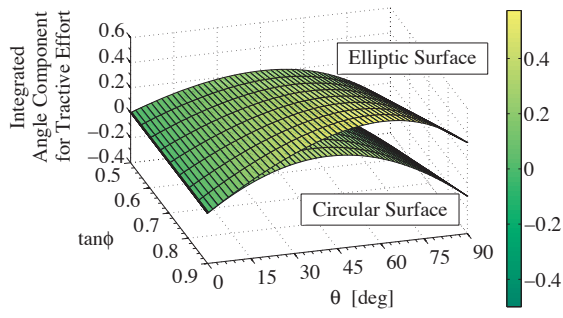
4.2 Advantage of Stresses on Elliptic Surface

Tractive components of the normal and the shear stresses acting on an elliptic surface is generally different from the ones on a circular surface. In the developed model, τ acts as $\tau \cos\xi$ and σ as $-\sigma \sin\xi$ for the tractive effort in x direction. On the other hand, τ acts as $\tau \cos\theta$ and σ as $-\sigma \sin\theta$ for a wheel. With consideration of Equation (20), the active angle component of the each stress for the tractive effort is shown in Figure 9. These results indicate the elliptic surface has an advantage over the circular one with smaller η . Furthermore, Figure 10 plots the ideal integrated angle components for the tractive efforts, $\int_0^\theta (\tan\phi \cos\theta - \sin\theta) d\theta$ and $\int_0^\xi (\tan\phi \cos\xi - \sin\xi) d\xi$. Here, the integrating components assume the available maximum shear stress of cohesionless soil in Equation (13), which is $\tau = \sigma \tan\phi$. The simulated plots indicate the elliptic surface works better than the circular surface. It is also confirmed that the ratio h/r becomes a critical factor for the genesis of the tractive effort.

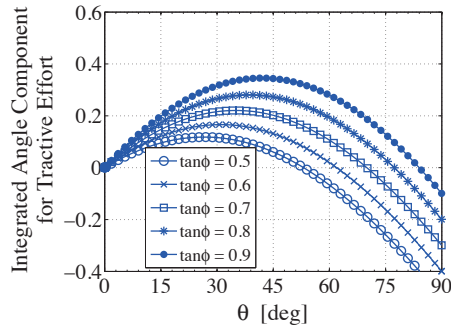
5 Simulation Analysis of Tractive Effort

5.1 Parameter Conditions

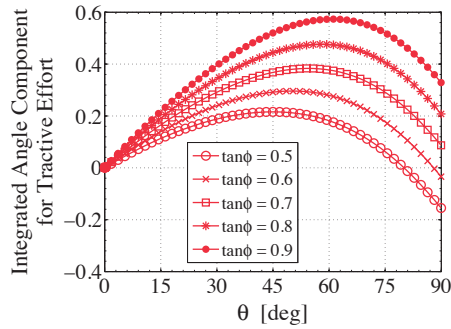
Through the simulations, the tractive effort F_x is calculated when Screw Driver Rover travels in a straight line. This provides $\delta = 0$ and $\alpha = 0$ as kinematic constraints. By reference to the experiments by Dugoff *et al.* [14], s_x is similarly set to be a variable parameter. With respect to the kinematic and geometric conditions, the nominal parameters are set: $N = 4$, $\eta = 5 \sim 30\text{deg}$, $r_1 = 0.035\text{m}$, $r_2 = 0.015\text{m}$, $h = 0.01 \sim 0.04\text{m}$ ($h_0 = 0.01\text{m}$), $\omega = \pm \frac{\pi}{2}\text{rad/s}$. Likewise, according to the experimental data targeting the sampled lunar soil [25] and the previous works [21], each soil parameter is set: $K = 0.018\text{m}$, $c = 0.17\text{kPa}$, $\phi = 35\text{deg}$, $c_1 = 0.4$, $c_2 = 0.15$, $c_3 = 0.2 \sim 0.8$,



(a) Comparative distributions



(b) Circular surface



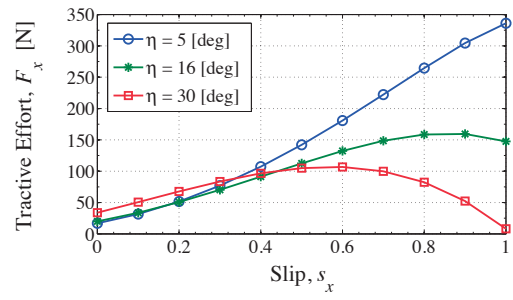
(c) Ellipse surface

Figure 10. Integrated angle components for tractive effort of normal and shear stresses

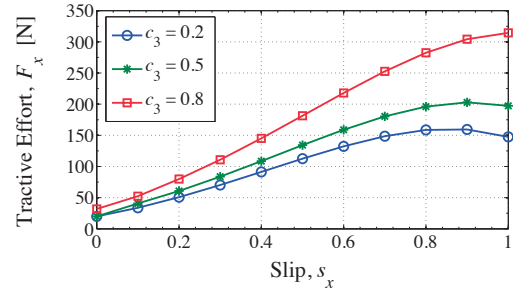
$c_4 = 0.01 \sim 0.03$, $n = 1.0$, $k_c = 1379\text{N/m}^{n+1}$ and $k_\phi = 814.4\text{kN/m}^{n+2}$.

5.2 Result and Discussion

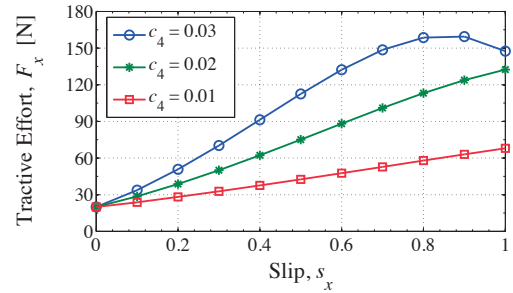
Figure 11 plots the simulation results performed by the proposed model. These results show the predicted tractive effort F_x with the slip s_x . According to these, it is confirmed F_x increases with an increase in s_x in most situations. This typical tendency was observed in the past experiments [12, 14], and therefore, this confirms the validity of the model. Next, Figure 11(a) indicates the slope angle η has little effect on F_x until $s_x = 0.5$. In contrast, an increase in η results in a pronounced increase in F_x under $s_x \gg 0.5$. From this, large sinkage induces a decrease of F_x . Moreover, Figure 11(b) shows the tendency that an in-



(a) With varying η , $c_3 = 0.2$ and $c_4 = 0.03$



(b) With varying c_3 , $\eta = 16\text{deg}$ and $c_4 = 0.03$



(c) With varying c_4 , $\eta = 16\text{deg}$ and $c_3 = 0.2$

Figure 11. Tractive effort and slip of Screw Drive Rover model with varying parameters

crease of the exit angle θ'_r introduces larger F_x . Although this indicates an increase of contact surface is significant, c_3 is unlikely to have a significant impact on F_x , compared to η . Further to these, Figure 11(c) shows the tendency that the sinkage h exerts an effect on F_x . With respect to h , F_x possesses a maximum value. Better understanding of c_4 is needed in the future work.

On the whole, the ratio of the sinkage and the radius h/r becomes one key factor in the light of Figure 10. The increase of the contact surface is expected to generate a larger F_x . However, the increase of h should be avoided even if the contact surface enlarges. An appropriate control of h/r is the most important technique for the enhancement of mobility performance of Screw Drive Rover on loose soil. So that Screw Drive Rover always generates positive tractive efforts, the design of η also becomes another important factor.

6 Conclusion

This paper presents the novel robot system using the Archimedean screw mechanism and its mathematical model for traveling on loose soil. The proposed model is developed based on the constructed terramechanics model with the screw geometry. Additionally, the soil shearing ellipse is newly employed, and then the shearing trajectory is represented three-dimensionally. In this paper the dependence of the model parameters is elaborated through the simulation analyses. Consequently, the advantage of the locomotion on loose soil by the screw units can be indicated. In particular, it is confirmed the screw units is an effective structure to avoid getting stuck.

As for future works, experimental validation is required to evaluate and grasp the detailed interaction of the soil and the screw unit. Further to this, the feedback from experiments to the model should be accomplished in order for enhancements of the model's feasibility.

References

- [1] S.W. Squyres *et al.*, "Two Years at Meridiani Planum: Results from the Opportunity Rover", *Science*, vol.313, no.5792, 2006, pp.1403-1407.
- [2] R.A. Kerr, "Mars Rover Trapped in Sand, But What Can End a Mission?", *Science*, vol.324, no.5930, 2009, p.998.
- [3] G.H. Heiken, D.T. Vaniman and B.M. French, *Lunar Sourcebook: A User's Guide to the Moon*, Cambridge University Press, MA, USA, 1991.
- [4] M.G. Bekker, *Introduction of Terrain-Vehicle Systems*, University of Michigan Press, MI, USA, 1969.
- [5] J.Y. Wong, *Theory of Ground Vehicles (3rd ed.)*, John Wiley & Sons, NY, USA, 2001.
- [6] T. Muro and J. O'Brien, *Terramechanics*, A.A. Balkema Publishers, Netherlands, 2004.
- [7] C.A. Pickover, "Mathematics and Beauty: A Sampling of Spirals and 'Strange' Spirals in Science, Nature and Art", *Leonardo*, vol.21, no.2, 1988, pp.173-181.
- [8] T. Koetsier and H. Blauwendraat, "The Archimedean Screw-Pump: A Note on Its Invention and the Development of the Theory", *Proc. 2004 Int. Symp. History of Machines and Mechanisms*, Cassino, Italy, 2004, pp.181-194.
- [9] T.J. Wells, "Buoyant Spiral Propeller", *U.S. Patent*, no.2400, Dec. 23th, 1841.
- [10] S.M. Code, "Amphibious Vehicle", *U.S. Patent*, no.1646611, Oct. 25th, 1927.
- [11] V. Asnani, D. Delap and C. Creager, "The Development of Wheels for the Lunar Roving Vehicle", *J. Terramech.*, vol.46, no.3 2009, pp.105-114.
- [12] S.J. Knight, E.S. Rush and B.G. Stinson, "Trafficability Tests with the Marsh Screw Amphibian", *J. Terramech.*, vol.2, no.4, 1965, pp.31-50.
- [13] M. Neumeyer and B. Jones, "The Marsh Screw Amphibian", *J. Terramech.*, vol.2, no.4, 1965, pp.83-88.
- [14] H. Dugoff and I. Ehrlich, "Model Tests of Buoyant Screw Rotor Configurations", *J. Terramech.*, vol.4, no.3, 1967, pp.9-22.
- [15] M.E. Rentschler *et al.*, "Modeling, Analysis, and Experimental Study of In Vivo Wheeled Robotic Mobility", *IEEE Trans. Rob.*, vol.22, no.2, 2006, pp.308-321.
- [16] M.E. Rentschler, S.M. Farritor and K. Iagnemma, "Mechanical Design of Robotic In Vivo Wheeled Mobility", *ASME J. Mech. Des.*, vol.129, no.10, 2007, pp.1037-1045.
- [17] M. Shikanai *et al.*, "Development of a Robotic Endoscope that Locomotes in the Colon with Flexible Helical Fins", *Proc. 31st Annual Int. Conf. IEEE/EMBS*, Minneapolis, MN, USA, 2009, pp.5126-5129.
- [18] A. Yamazaki *et al.*, "Three-Dimensional Analysis of Swimming Properties of a Spiral-Type Magnetic Micro-Machine", *Sens. Act. A*, vol.105, no.1, 2003, pp.103-108.
- [19] K. Nagaoka *et al.*, "Development of Lunar Exploration Rover Using Screw Propulsion Units: Note on Dynamic Behavior and Moving Direction Control", *Proc. 19th Workshop on JAXA Astrodyn. Flight Mech.*, Kanagawa, Japan, 2009, pp.143-148.
- [20] D.A. Crolla and A.S.A. El-Razaz, "A Review of the Combined Lateral and Longitudinal Force Generation of Tyres on Deformable Surfaces", *J. Terramech.*, vol.24, no.3, 1987, pp.199-225.
- [21] K. Iagnemma and S. Dubowsky, *Mobile Robots in Rough Terrain*, Springer, NY, USA, 2005.
- [22] Z.J. Janosi and B. Hanamoto, "The Analytical Determination of Drawbar Pull as a Function of Slip for Tracked Vehicle", *Proc. 1st Int. Conf. on Terrain-Vehicle Sys.*, Turin, Italy, 1961, pp.707-736.
- [23] O. Onafeko and A.R. Reece, "Soil Stresses and Deformations beneath Rigid Wheels", *J. Terramech.*, vol.4, no.1, 1967, pp.59-80.
- [24] J. Yamakawa, O. Yoshimura and K. Watanabe, "Development of Tire Model on Dry Sand by Model Size Experiment (First Report)", *Trans. Soc. Automotive Eng. Jpn.*, vol.39, no.6, 2008, pp.41-46. (in Japanese)
- [25] B.E. Wallace and N.S. Rao, "Engineering Elements for Transportation on the Lunar Surface", *Appl. Mech. Rev.*, vol.46, no.6, 1993, pp.301-312.